XII International Conference on Computational Plasticity. Fundamentals and Applications
COMPLAS XII
E. Oñate, D.R.J. Owen, D. Peric and B. Suárez (Eds)

CHARACTERIZATION AND MODELING OF VISCOELASTIC INTERFACE

L. ROULEAU[†,††], J.-F. DEÜ[†,*], A. LEGAY[†] AND F. LE LAY[††]

[†,*] Structural Mechanics and Coupled Systems Laboratory
Conservatoire national des arts et mtiers
292 Rue Saint-Martin
75141 Paris cedex 03, France
e-mail: lucie.rouleau, jean-francois.deu, antoine.legay@cnam.fr - web page:
http://www.lmssc.cnam.fr/en

[††] CESMAN - DCNS Research
44620 La Montagne, France
e-mail: frederique.le-lay@dcnsgroup.com - Web page: http://en.dcnsgroup.com/

Key words: Viscoelasticity, Kramers-Kronig relations, interface element, optimization

Abstract. Viscoelastic materials are commonly used as constrained thin layers in order to reduce the noise radiated by vibrating structures. The optimal design and placement of these viscoelastic interfaces requires an efficient characterization and modeling strategy. This work present an original automatic procedure to build the master curves of viscoelastic materials consistent with the causality principal, and interface finite elements for the modeling of thin constrained layers.

1 INTRODUCTION

Viscoelastic materials are extensively used in the automotive, aeronautic and naval industries for their damping properties. For instance, they are introduced as constrained thin layers in some parts of submarines in order to reduce the noise radiated by vibrating structures, and thus ensure stealthiness capabilities. The optimal design and placement of these viscoelastic interfaces requires an efficient characterization and modeling strategy adapted to parametric studies. Firstly, an original automatic procedure to build the master curves of viscoelastic materials from measurements using dynamic mechanical analysis, based on the Kramers-Kronig causality relations is developed. Secondly, a zero-thickness interface finite element is formulated to model the thin constrained viscoelastic layer.

2 CHARACTERIZATION OF VISCOELASTIC MATERIALS

Mechanical properties of viscoelastic materials exhibit a strong dependence on frequency and temperature [1] and are commonly described using a complex modulus approach:

$$G^*(\omega, T) = |G(\omega, T)| \mathrm{e}^{\mathrm{i}\phi(\omega,T)} \tag{1}$$

Dynamical mechanical analysis (DMA) allows the measurement of the amplitude $|G(\omega, T)|$ and the loss angle $\phi(\omega, T)$ at different frequencies and temperatures. The measurable frequency range being limited, the time-temperature superposition principle is applied. It states that the viscoelastic behaviour at a temperature T_0 can be related to that at another temperature T by multiplying the frequency scale by a shift factor a_T, and the modulus' amplitude by a shift factor b_T. These shift factors depend on the temperatures T_0 and T [1]:

$$\begin{aligned} |G(f, T)| &= b_\mathrm{T}(T, T_0)|G(f_r, T_0)| \\ f_r &= a_\mathrm{T}(T, T_0) f \end{aligned} \tag{2}$$

where f is the frequency of measurement and f_r is the reduced frequency after application of the shift factors. Figure 1 illustrates the time-temperature superposition principle. Shift coefficients a_T et b_T are commonly determined using a least square method aiming at the best superposition of the shifted isotherms [2]. However, this technique does not give any physical meaning to the shift coefficients. Other methods make use of viscoelastic models to determine the shift factors [3]. This way, the calculated shift coefficients have a physical meaning since the viscoelastic model is supposed to verify some conditions such as causality and thermodynamic principles. But it requires to set a priori the material modulus function. If the chosen viscoelastic model is not the most appropriate to model the frequency dependence of the mechanical properties of the viscoelastic material, it may lead to significant discrepancies between the experiments and the model. The goal of section 2.1 is to present the developed method to optimize the shift coefficients according to the causality principle [4]. The method is applied to DMA measurements of Deltane 350, an amorphous polymer from Paultra®, and results are given in section 2.2.

2.1 Automatic shifting procedure for construction of master curves

In the context of linear viscoelasticity, the causality principle imposes relationships between the amplitude and the loss angle of the complex modulus, called Kramers-Kronig relations [5]:

$$\begin{cases} \ln(|G^*(\omega)|) = & \ln(|G_\infty|) + \dfrac{2}{\pi} \displaystyle\int_0^\infty \dfrac{u\phi(u)}{\omega^2 - u^2} \mathrm{d}u \\ \phi(\omega) = & \dfrac{2\omega}{\pi} \displaystyle\int_0^\infty \dfrac{\ln(|G^*(u)|)}{u^2 - \omega^2} \mathrm{d}u \end{cases} \tag{3}$$

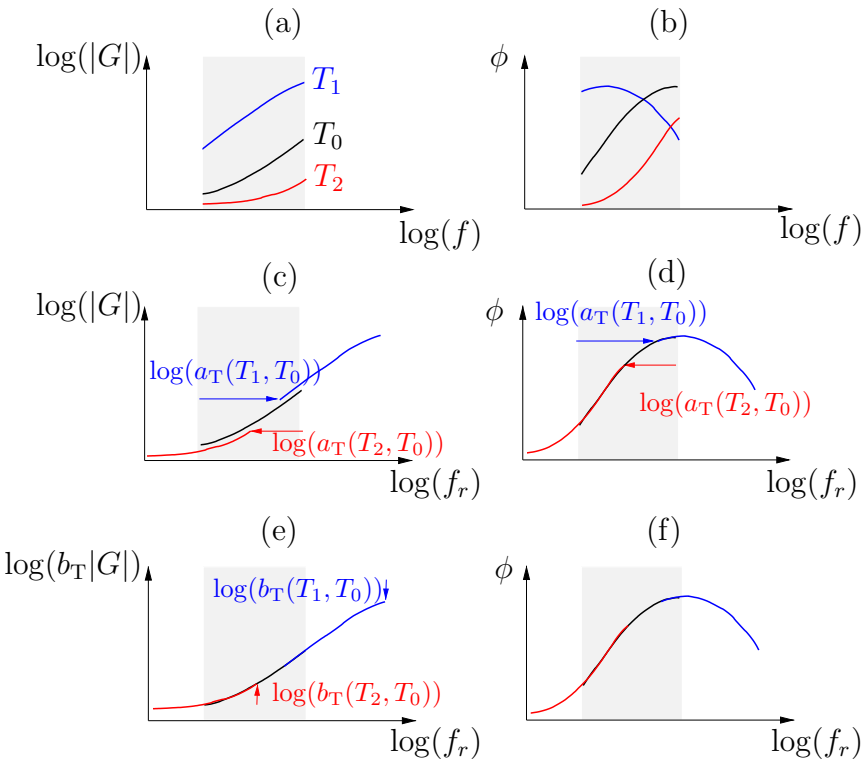

Figure 1: Time-temperature superposition principle. (a), (b) Isotherms of the complex modulus amplitude and the phase angle on a limited frequency range with $T_1 < T_0 < T_2$. (c), (d) Horizontal shifting of the isotherms of complex modulus amplitude and the phase angle with T_0 the reference temperature. (e), (f) Vertical shifting of the isotherms of complex modulus amplitude with T_0 the reference temperature.

where G_∞ is the unrelaxed modulus ($G_\infty = G^*(\omega \to \infty)$). The optimization procedure proposed in this work aims at determining shift factors that produce master curves consistent with the Kramers-Kronig relations. Experimental measurements of the amplitude and the loss angle of the complex modulus are performed on the frequency range $\mathbf{f} = [f_1, f_2, \ldots, f_{n_\mathrm{f}}]$ and on the temperature range $\mathbf{T} = [T_1, T_2, \ldots, T_{n_\mathrm{T}}]$. This leads to a cloud of $n = n_\mathrm{T} \times n_\mathrm{f}$ measurement points. During a first step of initialization, the shift coefficients b_T are set to unity, and the shift coefficients a_T are those obtained by a least square method. The second step consists in determining the set of parameters $\mathbf{x} = [a_\mathrm{T}(\mathrm{T}_1), \ldots, a_\mathrm{T}(\mathrm{T}_{n_\mathrm{T}}), b_\mathrm{T}(\mathrm{T}_1), \ldots, b_\mathrm{T}(\mathrm{T}_{n_\mathrm{T}})]$ minimizing a cost function $\mathbf{F}$, representing the discrepancies between the experimental shifted modulus and the modulus computed by the Kramers-Kronig relations :

$$[\mathbf{a}_\mathrm{T}^\mathrm{opt}, \mathbf{b}_\mathrm{T}^\mathrm{opt}] = \left\{ \mathbf{x} \left| \min_{\mathbf{x}} \left(\sum_{i=1}^{n_f} |\mathbf{F}(\mathbf{x}, f_\mathrm{r}^i)|^2 \right) \right. \right\} \tag{4}$$

For a given set of parameters $\mathbf{x} = [a_\mathrm{T}(\mathrm{T}_1), \ldots, a_\mathrm{T}(\mathrm{T}_{n_\mathrm{T}}), b_\mathrm{T}(\mathrm{T}_1), \ldots, b_\mathrm{T}(\mathrm{T}_{n_\mathrm{T}})]$, the time-temperature superposition principle is applied to experimental data, in order to obtain shifted data:

$$\begin{aligned} &f_\mathrm{r}^i = a_\mathrm{T}(T_j) f_k \\ &\ln(|G^*_\mathrm{shift}(\mathbf{x}, f_\mathrm{r}^i(\mathbf{x}))|) = \ln(b_\mathrm{T}(T_j)) + \ln(|G^*_\mathrm{exp}(T_j, f_k)|) \\ &\phi_\mathrm{shift}(\mathbf{x}, f_\mathrm{r}^i(\mathbf{x})) = \phi_\mathrm{exp}(T_j, f_k) \end{aligned} \tag{5}$$

where $i = 1 \ldots n$, $j = 1 \ldots n_\mathrm{T}$ and $k = 1 \ldots n_\mathrm{f}$. The functions $\ln(|G^*_\mathrm{shift}|)$ and ϕ_shift are first smoothed and extended on the interval $[0, +\infty[$ (denoted $\ln(|G^*_\mathrm{int}|)$ and ϕ_int hereafter), then numerically integrated in the Kramers-Kronig relations according to the method described in [6]:

$$\begin{aligned} \ln(|G^*_\mathrm{KK}(\mathbf{x}, f_\mathrm{r})|) &= \ln(|G^*_{\mathrm{int}\ \infty}|) + \frac{2}{\pi} \int_0^\infty \frac{u \phi_\mathrm{int}(\mathbf{x}, u)}{f_\mathrm{r}^2 - u^2} \mathrm{d}u \\ \phi_\mathrm{KK}(\mathbf{x}, f_\mathrm{r}) &= \frac{f_\mathrm{r}}{\pi^2} \int_0^\infty \frac{\ln(|G^*_\mathrm{int}(\mathbf{x}, u)|)}{u^2 - f_\mathrm{r}^2} \mathrm{d}u \end{aligned} \tag{6}$$

Exact verification of the Kramers-Kronig relations corresponds to $\ln(G^*_\mathrm{KK}) = \ln(G^*_\mathrm{shift})$. The cost function to be minimized is defined as:

$$\begin{aligned} \mathbf{F}(\mathbf{x}, f_\mathrm{r}^i) =& \frac{\ln(G^*_\mathrm{shift}(\mathbf{x}, f_\mathrm{r}^i(\mathbf{x}))) - \ln(G^*_\mathrm{KK}(\mathbf{x}, f_\mathrm{r}^i(\mathbf{x})))}{\ln(G^*_\mathrm{shift}(\mathbf{x}, f_\mathrm{r}^i(\mathbf{x})))} \\ =& \frac{\ln(|G^*_\mathrm{shift}(\mathbf{x}, f_\mathrm{r}^i(\mathbf{x}))|) + \mathrm{i}\phi_\mathrm{shift}(\mathbf{x}, f_\mathrm{r}^i(\mathbf{x}))}{\ln(|G^*_\mathrm{shift}(\mathbf{x}, f_\mathrm{r}^i(\mathbf{x}))|) + \mathrm{i}\phi_\mathrm{shift}(\mathbf{x}, f_\mathrm{r}^i(\mathbf{x}))} \\ & - \frac{\ln(|G^*_\mathrm{KK}(\mathbf{x}, f_\mathrm{r}^i(\mathbf{x}))|) + \mathrm{i}\phi_\mathrm{KK}(\mathbf{x}, f_\mathrm{r}^i(\mathbf{x}))}{\ln(|G^*_\mathrm{shift}(\mathbf{x}, f_\mathrm{r}^i(\mathbf{x}))|) + \mathrm{i}\phi_\mathrm{shift}(\mathbf{x}, f_\mathrm{r}^i(\mathbf{x}))} \end{aligned} \tag{7}$$

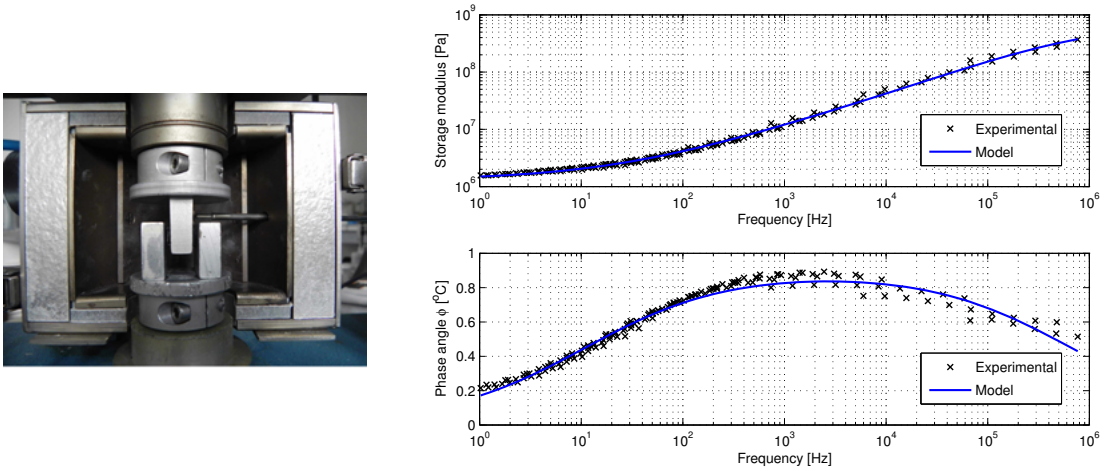

(a) (b)

Figure 2: DMA Metravib 450+ in a shear mode configuration (a) and master curves of Deltane 350 at the reference temperature $T_0 = 12^o$C (b).

2.2 Application of the method to Deltane 350

Deltane 350 is used for validation of the method described above. It is an amorphous polymer from Paulstra®, commonly used in aeronautic applications. DMA measurements are carried out on a Metravib DMA 450+ with the testing configuration in the shear mode (figure 2a). The specimen are tested on the frequency range5Hz - 400Hz ($n_\mathrm{f} = 10$ measurement points) and over the temperature range -40^oC - 43^oC ($n_\mathrm{T} = 18$ measurement points). A dynamic displacement of 5μm is applied to the specimen to remain in the linear viscoelasticity domain.

The procedure presented above is applied to the DMA measurements for Deltane 350 to build the master curves at the reference temperature $T_0 = 12^o$C (Figure 2b). The initialized and optimized shift coefficients are plotted on Figure 3 and 4. The final shift coefficients calculated are in accordance with the Williams-Landel-Ferry equation [1] and the Bueche-Rouse theory [7].

3 Modeling of viscoelastic interfaces

For thin structures or structures with simple geometry, the viscoelastic interface can be modeled by sandwich beam/plate/shell elements [8, 9]. However for structures that do not fall into this category, 3D finite elements are required. Hence, a change in the thickness or the placement of the viscoelastic layer imply a complete re-meshing of the structure. The calculation of new stiffness and mass matrices for each set of structural parameter represents an additional significant computational cost in a parametric study. In this section is presented the formulation of a new interface finite element to model the

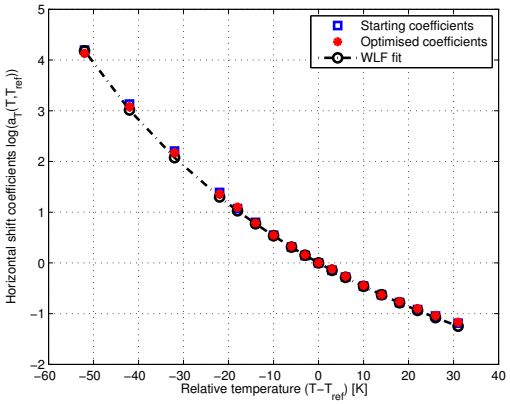

Figure 3: Initialized and optimized shift factors a_{T} compared to the shift factors a_{T} predicted by the Williams-Landel-Ferry equation [ref].

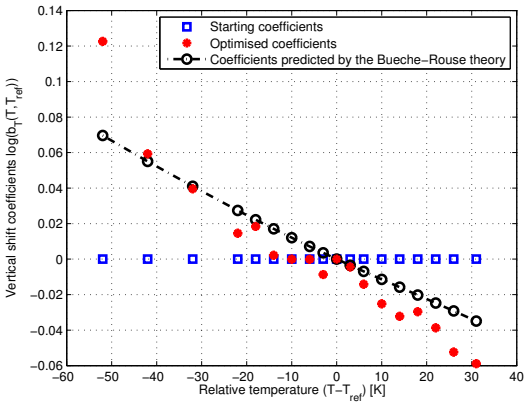

Figure 4: Initialized and optimized shift factors b_{T} compared to the shift factors b_{T} predicted by the Bueche-Rouse theory [ref].

viscoelastic interface [10] which is then compared with 3D elements.

3.1 Element formulation

The interface element is a 12-nodes wedge-shape element connecting two quadratic tetrahedra, as shown on Figure 5. The two triangular surfaces of the interface element lie together in the initial configuration so that the initial thickness is zero. The interface element is then characterized by a surface and a fictive thickness h which is assumed to remain constant (see Figure 6). Each node i has three degrees of freedom: U_x^i, U_y^i and U_z^i, the nodal displacement in the global coordinate system (x, y, z). The three-dimensional field (u_x, u_y, u_z) is approximated by:

$$\begin{bmatrix} u_x \\ u_y \\ u_z \end{bmatrix} = \begin{bmatrix} \mathbf{N} & \mathbf{0} & \mathbf{0} \\ \mathbf{0} & \mathbf{N} & \mathbf{0} \\ \mathbf{0} & \mathbf{0} & \mathbf{N} \end{bmatrix} \begin{bmatrix} \mathbf{U}_x \\ \mathbf{U}_y \\ \mathbf{U}_z \end{bmatrix} = \mathbb{N}\mathbf{U} \tag{8}$$

where $\mathbf{N}$ is the vector of shape functions for a 12-nodes wedge finite element. The Jacobian matrix of the transformation from the reference coordinate system (r, s, t) to the global coordinate system is calculated as:

$$\mathbf{J} = \begin{bmatrix} \frac{\partial x}{\partial r} & \frac{\partial x}{\partial s} & \frac{\partial x}{\partial t} \\ \frac{\partial y}{\partial r} & \frac{\partial y}{\partial s} & \frac{\partial y}{\partial t} \\ \frac{\partial z}{\partial r} & \frac{\partial z}{\partial s} & \frac{\partial z}{\partial t} \end{bmatrix} = \begin{bmatrix} \frac{\partial \mathbf{N}}{\partial r}\mathbf{X}^{\mathrm{f}} & \frac{\partial \mathbf{N}}{\partial s}\mathbf{X}^{\mathrm{f}} & \frac{\partial \mathbf{N}}{\partial t}\mathbf{X}^{\mathrm{f}} \\ \frac{\partial \mathbf{N}}{\partial r}\mathbf{Y}^{\mathrm{f}} & \frac{\partial \mathbf{N}}{\partial s}\mathbf{Y}^{\mathrm{f}} & \frac{\partial \mathbf{N}}{\partial t}\mathbf{Y}^{\mathrm{f}} \\ \frac{\partial \mathbf{N}}{\partial r}\mathbf{Z}^{\mathrm{f}} & \frac{\partial \mathbf{N}}{\partial s}\mathbf{Z}^{\mathrm{f}} & \frac{\partial \mathbf{N}}{\partial t}\mathbf{Z}^{\mathrm{f}} \end{bmatrix}, \tag{9}$$

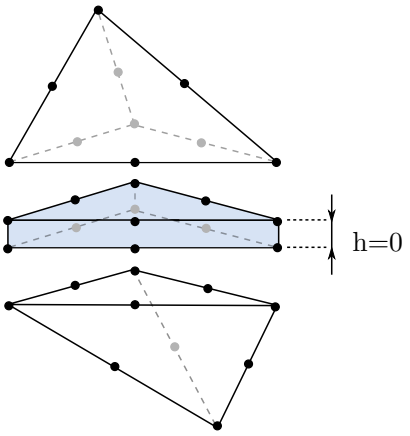

Figure 5: Interface finite element connected to quadratic tetrahedra in the initial configuration.

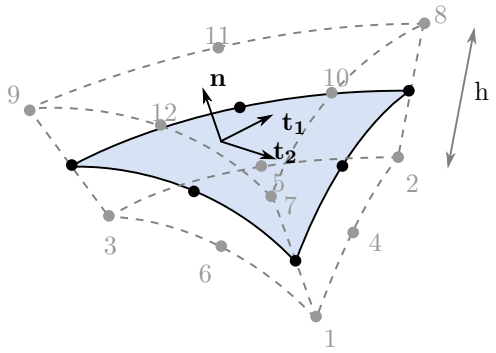

Figure 6: Interface finite element showing its characterizing mean surface and fictive thickness h.

where $[\mathbf{X}^{\mathrm{f}}, \mathbf{Y}^{\mathrm{f}}, \mathbf{Z}^{\mathrm{f}}]^T = [\mathbf{X}, \mathbf{Y}, \mathbf{Z}]^T \pm \dfrac{h}{2}\mathbf{n}$ are the coordinates of the fictive nodes obtained from the coordinates of the physical nodes $[\mathbf{X}, \mathbf{Y}, \mathbf{Z}]^T$ after calculation of the normal $\mathbf{n}$ to the mean surface at each node. The elementary stiffness and mass matrices are defined as:

$$\begin{aligned} \mathbb{K}_v &= \int_{V_e} \mathbb{B}^T \mathbb{C}^*(\omega) \mathbb{B} \det(\mathbf{J}) \mathrm{d}V \\ \mathbb{M}_v &= \int_{V_e} \mathbb{N}^T \rho \mathbb{N} \det(\mathbf{J}) \mathrm{d}V \end{aligned} \tag{10}$$

with $\mathbb{B}$ is the discretized gradient matrix, V_e is the volume of the element in the reference coordinate system, ρ is the density of the viscoelastic material and $\mathbb{C}$ is the elasticity matrix which can be written as:

$$\mathbb{C}^*(\omega) = G^*(\omega) \begin{bmatrix} \dfrac{2(1-\nu)}{1-2\nu} & \dfrac{2\nu}{1-2\nu} & \dfrac{2\nu}{1-2\nu} & 0 & 0 & 0 \\ \dfrac{2\nu}{1-2\nu} & \dfrac{2(1-\nu)}{1-2\nu} & \dfrac{2\nu}{1-2\nu} & 0 & 0 & 0 \\ \dfrac{2\nu}{1-2\nu} & \dfrac{2\nu}{1-2\nu} & \dfrac{2(1-\nu)}{1-2\nu} & 0 & 0 & 0 \\ 0 & 0 & 0 & 1 & 0 & 0 \\ 0 & 0 & 0 & 0 & 1 & 0 \\ 0 & 0 & 0 & 0 & 0 & 1 \end{bmatrix} \tag{11}$$

where ν is the Poisson ratio, which is assumed to remain constant. The integration of the elementary matrices $\mathbb{K}_v$ and $\mathbb{M}_v$ over the volume V_e makes use of 12 quadrature points, considering two quadrature points in the through-thickness direction.

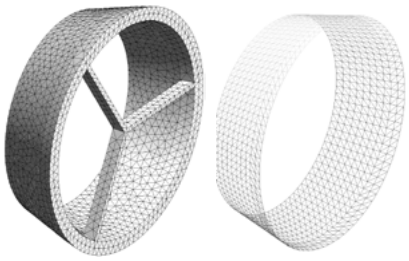

Figure 7: Mesh of the three-dimensionnal structure to be damped and definition of the mean surface of interface elements modeling the viscoelastic constraining layer.

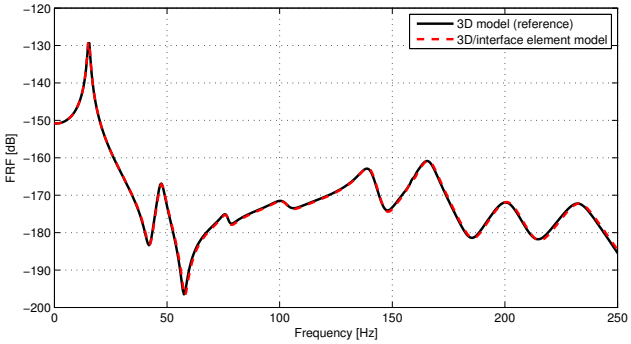

Figure 8: Frequency response function of the damped structure on the interval $[0, 250]$ Hz, with a frequency step of 0.5Hz, for a constrained damping layer modelled by quadratic tetrahedra (solid line) and by interface finite elements (dashed line).

3.2 Element validation

The interface element is validated by calculating the frequency response function of the structure shown on Figure 7, where CLD treatment is applied at the core of the cylindrical part. The thickness of the damping layer represents about 1/50 of the total thickness of the structure. The elastic structure is made of steel ($E = 2.1e11$ Pa, $\nu = 0.3$, $\rho = 7800$ kg/m^3) and the viscoelastic material used for damping is Deltane 350. The frequency dependent properties of Deltane 350 are represented by a fractional derivative model:

$$G^*(\omega) = \frac{G_0 + G_\infty(\mathrm{i}\omega\tau)^\alpha}{1 + (\mathrm{i}\omega\tau)^\alpha}, \tag{12}$$

whose parameters are identified on the experimental master curves obtained in the first section:

$$G_0 = 1.29 \text{ MPa} \qquad G_\infty = 0.72 \text{ GPa} \qquad \tau = 0.24\ \mu\text{s} \qquad \alpha = 0.5 \tag{13}$$

The identified fractional derivative model gives a good representation of the mechanical properties of the viscoelastic material, as shown on Figure 2b.

The damped structure, which aims at representing a turbine nozzle, is fixed at the intersection of the radial stiffeners and a unit load is applied. Quadratic tetrahedra are used to model the 3D structure while interface finite elements model the damping layer.

The calculated frequency response is compared to the one obtained by modelling the viscoelastic layer with 3D finite elements. Figure 8 shows that both curves are practically superposed, thus validating the interface finite element previously formulated.

4 CONCLUSIONS

The shifting procedure proposed to calculate the shift coefficients when applying the time-temperature superposition principle makes use of the Kramers-Kronig relations. The determined shift coefficients are found to be in accordance with the WLF equation and the Bueche-Rouse theory. They produce master curves which are consistent with the causality condition.

A 12-nodes interface finite element has been formulated and programmed to model thin constrained viscoelastic layers. This element can be connected to quadratic tetrahedra, which allows the modelling of structures with complex geometry, and gives equivalent results to a three-dimensional representation of the damping layer. Since the interface element is characterized by a mean surface and a fictive thickness, no re-meshing is necessary to test several positions or thickness of the viscoelastic layer, and so the stiffness and mass matrices of the elastic structure need only to be locally updated.

The proposed characterizing and modeling strategy is appropriate for parametric studies.

REFERENCES

[1] J.D. Ferry. *Viscoelastic properties of polymers*, John Wiley & Sons, 1980.

[2] 01dB-Metravib. *Dynatest User Manual DYNATEST.06/NUT/002/B.*

[3] R.M. Guedes. *A viscoelastic model for a biomedical ultra-high molecular weight polyethylene using the time-temperature superposition principle*, Polymer testing, 30, 294-302, 2011.

[4] L. Rouleau, J.-F. Deü, A. Legay, F. Le Lay. *Application of Kramers-Kronig relations to time-temperature superposition for viscoelastic materials*, submitted to Mechanics of Materials in November 2012.

[5] H.A. Kramers, *La diffusion de la lumière par les atomes*, In Atti del Congresso Internazionale dei Fisici, 1927.

[6] J.-M. Parot, B. Duperray. *Applications of exact causality relationships to materials dynamic analysis*, Mechanics of Materials, 39, 419-433, 2007.

[7] F. Bueche. *The viscoelastic properties of plastics*, Journal of Chemical Physics, 22, 603-609, 1954.

[8] E. Carrera. *Historical review of zigzag theories for multilayered plates and shells*, Applied Mechanical Review, 56, 287-308, 2003.

[9] J.-D. Chazot, B. Nennig, A. Chettah *Harmonic response computation of viscoelastic multilayered structures using a ZPST shell element*, Computers and Structures, 89, 2522-2530, 2011.

[10] Rouleau, L., Deü, J.-F., Legay, A., Le Lay, F.. Caractérisation et modélisation d'interfaces viscoélastiques. In: *Proceedings of the 11ème Colloque National en Calcul des Structures*, Giens, France, 13-17 May 2013.